Jordanian Journal of Computers and Information Technology (JJCIT), Vol. 07, No. 03, September 2021.

A HYPER-SURFACE-BASED MODELING AND CORRECTION OF BIAS FIELD IN MR IMAGES

Daouia Azzouz[1] and Smaine Mazouzi[2]

(Received: 29-Mar.-2021, Revised: 16-May-2021, Accepted: 25-May-2021)

ABSTRACT

Dealing with the different artifacts in medical images is necessary to perform several tasks, including segmentation. We introduce in this paper a novel method for bias field correction in Magnetic Resonance Imaging (MRI). Using the segmentation results obtained by a modified Expectation Maximization clustering, the bias field is fitted as a hyper-surface in a 4D hyper-space. Then, it is corrected based on the fact that voxels belonging to the same tissue should have the same intensity in the whole image. So, after a quick and coarse unsupervised voxel labeling by clustering by parts is performed, the bias field is computed for reliably labeled voxels. For the less reliably labeled voxels, the bias field is interpolated using a hyper-surface, estimated by a 4D Lagrangian interpolation. We evaluated the efficiency of the proposed method by comparing segmentation results with and without bias field correction. Also, we used the coefficient of variation within the MRI volume. Segmentation results and the coefficient of variation results were significantly enhanced after bias field correction by the proposed method.

KEYWORDS

MRI data labeling, Bias field correction, EM clustering, 4D hyper-surface, Lagrangian interpolation.

1. INTRODUCTION

One of the specific artifacts in Magnetic Resonance Imaging (MRI) is the Intensity Non-Uniformity (INU) across the data volume. This artifact consists in a slow and smooth variation of the intensity, whereas it should be the same for all the voxels in the same tissue. The Intensity Non-Uniformity (INU) is caused by several combined factors, the two main of which are the lack of sensitivity of the radio-frequency (RF) of the coils and the attenuation of the RF signal inside the tissues [29]. The challenge in such a problem is that it cannot be considered as a conventional additive Gaussian noise that can be efficiently removed by denoising methods. So, the intensity non-uniformity, produced as a bias field, is a full hard problem and thus it requires specific methods for estimation and correction. Methods for image segmentation or image registration must take into account the bias field and deal with it in order to provide reliable processing results. Some of these methods proceed by jointly, correcting the bias field and segmenting or registering images [4], [27], [6], [8], [13]. Nevertheless, most of them consider the bias field correction as a pre-processing task that precedes the segmentation or the registration [5], [16], [13]. The hardness of the problem lies in the fact that the intensity variation caused by the bias field is very slow and so, it is hard to detect locally.

We propose in this paper a novel method for bias field correction in MR images, based on a quick and coarse segmentation of MR data. Using the resulting segmentation, a hyper-surface in a 4D space, that models the bias field in the whole 3D image volume, is fitted using a Lagrangian interpolation. First, a modified EM (Expectation Maximization)-based clustering is performed on a set of sub-volumes, covering the entire volume of the image. So, the obtained labeling results in the different sub-volumes are merged in order to obtain the segmentation of the whole volume. Such an EM-clustering by parts allows to reduce false voxel labeling that occurs when the clustering is performed in the whole volume. The labeling in the whole volume results in three sets of voxels, corresponding respectively to the three tissues of interest of the brain matter; namely: Cerebro-Spinal Fluid (CSF), Gray Matter (GM) and White Matter (WM). Then, only the voxels with high membership certainty (most confidently labeled) are used to estimate the bias field at their respective positions in the image. Using the estimated bias field values at the reliably labeled voxels, a 4D hyper-surface is fitted in the 4D hyper-space (X,Y,Z,I), using a 4D Lagrangian surface [38]. Based on the fitted hyper-surface, the bias field is calculated for the remainder of the less reliably labeled voxels and so, the intensity can be corrected in the whole image. According

D. Azzouz[1] and S. Mazouzi[2] are with University 20 Aout 1955, Skikda, Alegria. Emails: [1]azzouz.daouia@gmail.com, [1]d.azzouz@univ-skikda.dz and [2]s.mazouzi@univ.skikda.dz.

to the literature, polynomial fitting was used several times to model the bias field [36], [34], [19]. However, on one hand, if the used polynomials are with low order, they do not well fit the bias field [19]. On the other hand, if the order of the used polynomials is high, such in polynomials, computation results in a combinatorial explosion of the number of parameters and therefore a prior knowledge must be provided in order to use low-order Legendre polynomials [34]. Unlike the state-of-the-art methods that use highly computational polynomials for the bias field surface fitting, our method is based on Lagrangian polynomial, where the order can be high, nevertheless the number of the involved parameters remains low.

Evaluating the performances of a method for bias field correction can be performed by comparing the segmentation results without and with bias correction, by using the same method of image segmentation [9]. It has been obtained that the bias field estimation and correction according to our method, using the proposed modified EM clustering algorithm, allows to significantly enhance the segmentation of MR images. Furthermore, the coefficient of variation (*CV*) has been used to show that the intensity homogeneity was enhanced for both the simulated and the real MRI involved in the experimentation.

The remainder of the paper is organized as follows: In Section 2, we introduce a short review of some well-referenced works in the literature, having dealt exclusively or jointly with bias field correction. Section 3 is devoted to the new method proposed in this work, where we show how a prior fast and coarse segmentation is performed using a modified EM-based clustering by parts, then how the bias field is firstly calculated for the reliably labeled voxels. In the remainder of the same section, we show how the bias field is fitted using a hyper-surface and how the image intensity is corrected. Section 4 is reserved for the experimentation of the proposed method, where we show and compare the segmentation results with and without bias field correction. Furthermore, the results of the coefficient of variation are computed and compared with those of other methods. It will be noted that the intensity was significantly enhanced in the involved MRI. In Section 5, we summarize the work and highlight some of its potential perspectives.

2. RELATED WORK

Several authors have proposed different methods for bias field correction in MR images. Some methods, in particular the earlier ones, were filtering-based [36]. For such methods, the bias field is removed by considering it as a low-frequency artifact, compared to high-frequency anatomic structures [24]-[25]. Filtering-based methods suffer from two common problems that lead to less accurate bias field removed and therefore to less efficient image post-processing: First, they significantly alter the image near the edges of the regions (Hallo effect), so that a special processing should be considered to preserve edge sharpness [2], [18]. Second, they erase low-frequency structures as a result of spatial blind filtering. To deal with this problem, some authors, such as those in [21], were able to preserve low-frequency structures by a combination of singularity functions. Following the same approach, the authors in [33] have applied homomorphism filtering for bias-field correction. Their method consists in extracting the log-bias by low-pass filtering, then the latter is subtracted from the log-image in order to obtain the log-corrected image. Aiming at preserving image details while the bias field is corrected, the authors in [8] remove the bias field by extracting image details after multi-layered Gaussian filtering.

Level set formulation was used by Li et al. for jointly correcting the bias field and segmenting the image [20]. By minimizing the level set functional that defines the clustering criterion, the segmentation of the image and the correction of the bias field are jointly performed. In another work, Chang et al. have proposed a new variation model for INU correction for Rodent Brain MRIs [7]. Based on Mumford–Shah functional, the authors define several terms to be minimized, aiming at extracting the bias mask. A morphological processing is also applied in order to enhance the obtained mask. Based on local and global information, Cong et al. proposed a novel model for MRI segmentation and INU correction [10]. Neighborhood information defines local constraints and the global regularization is performed based on global spatial information. In a recent work, Shan et al. [28] proposed a region-based active contour model with interleaved image segmentation and INU correction. A global energy functional, which was obtained by combining local energies, is fitted thanks to a level set method, where two regularization terms allow to fit the image energy functional.

Other authors have assumed that the intensity of a given tissue does not change in the whole image unless because of the bias field. So, the bias field is estimated as the intensity variation within the same

type of tissue. This variation is often represented by a surface that must be fitted, often by B-spline approximations. In [22], the authors use a second-order polynomial to model the intensity within a dominant tissue, automatically extracted. A Gaussian model of the dominant tissue was beforehand proposed in [35]. The main drawback of such methods is that they were designed for a dominant tissue. For the other tissues, the bias field is not or at most roughly estimated. In [32], the bias field was taken into account in the similarity measurement that allows to enhance the separability of MRI data. Moreover, the formulated objective function of the Fuzzy C-Means (FCM) algorithm integrates a regularization term that compensates the bias field. Meena Prakash et al. have combined the FCM algorithm and Expectation-maximization (EM) algorithm for brain MRI segmentation with bias correction [26]. In their implementation, they take into account the spatial information, by incorporating it by convolution of the posterior probability during E-Step of the EM algorithm. Mishro et al. have also opted for fuzzy clustering for INU correction in brain MRIs [23]. They also incorporate spatial information by altering the membership matrix of standard FCM, aiming to attenuate the effect of noise and INU. So, equidistant pixels are assigned to a single cluster.

Recently, machine leaning-based methods for INU correction started to be proposed. Dai et al. [11] proposed a deep learning-based INU correction algorithm, called residual cycle generative adversarial network (res-cycle GAN), which consists of the calculation of the inverse transformation between the INU uncorrected and corrected MRIs; so it will be possible to compute the INU corrected MRIs.

3. PRIOR SEGMENTATION AND BIAS FIELD ESTIMATION AND CORRECTION

We remind that the bias field, which consists in a non-uniformity of the intensity of the magnetic field, causes a slow and smooth variation of the luminance within MR images. This artifact leads to erroneous results of image segmentation, because voxels belonging to a same tissue could have significantly different intensities, especially if they are far from each other (see Figure 1). In order to correct the intensity in the raw image, the bias field must be estimated. In this work, a 4D hyper-surface is fitted in order to model the bias field in the whole 3D image. The principle of the proposed method consists to asses that in a small region, after it is smoothed to reduce the noise within, voxels should have the same average intensity if they belong to the same type of tissue. According to this principle, we proceed by segmenting small sub-volumes in the MRI, where we can assume that the intensity variation due to the bias field can be neglected. Then, the segmentation of the whole MRI is obtained by the fusion of the different sub-segmentations. So, as the segmentation is assumed correct, the bias field at a given voxel is expressed by the ratio between the intensity of the voxel and the intensity of a selected voxel, called voxel of reference that belongs to the same tissue as the voxel in question. Such an assumption is based on the following model that expresses how the true image I was altered by the bias field β and affected by a Gaussian noise η, resulting in the measured image $\hat{I}$.

$$I(x,y,z) = (I(x,y,z) + \eta(x,y,z)) \times \beta(x,y,z) \quad (1)$$

So, the main stages for bias estimation and intensity correction according to our method are as follows: First, a voxel labeling is performed by an EM-based clustering algorithm that is executed separately on several sub-volumes. Then, the results of voxel labeling in the different sub-volumes are merged. Such a local clustering avoids to gather voxels that belong to a given same tissue, but have different intensities because they are far from each other. Note that a global clustering that involves the whole 3D volume results in a high rate of erroneous voxel labeling, in particular when the bias field level is high (see Figure 1). So, we introduce in sub-section 3.1 a new iterative EM-based algorithm for voxel labeling. The algorithm generates random sub-volumes within the MRI volume, where the bias field at each sub-volume is low, what allows sufficiently reliable voxel labeling. After the voxels in the whole volume are labeled according to a given merge scheme, the bias field is estimated first for the set of the voxels that are reliably labeled, according to their membership certainty. Then, for each connected set of less-reliably labeled voxels, where the bias was not calculated, a cuboid is set, in which a 4D hyper-surface will be fitted. Control points used to fit the hyper-surface are the voxels in the cuboid where the bias field was calculated. Finally, the bias field at the less reliably labeled voxels in the cuboid is interpolated using the fitted hyper-surface (see Figure 2).

3.1 Voxel Labeling by Iterative EM Clustering by Parts

We assume that MR images are skull-striped, using a brain extractor tool, such as BET of FSL [30],

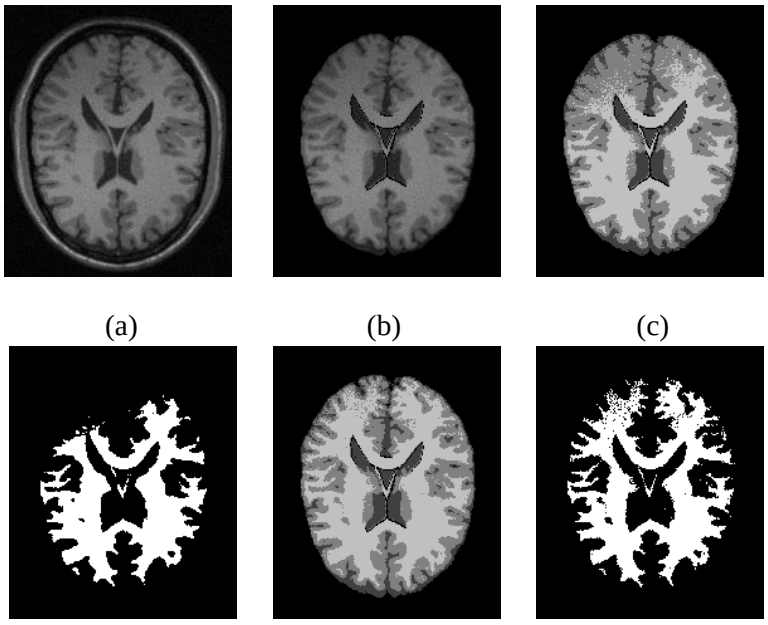

Figure 1. Erroneous labeling with presence of high INU: a) Raw MRI with 3% noise level and 90% INU level; b) Extracted brain tissues; c) Global EM clustering results, where we can notice the strong alteration of the white matter at the top of the image which was erroneously labeled as gray matter; d) Extracted white matter, where an important part at the top is truncated; e) Voxel labeling by the modified EM by parts algorithm; f) Resulting white matter.

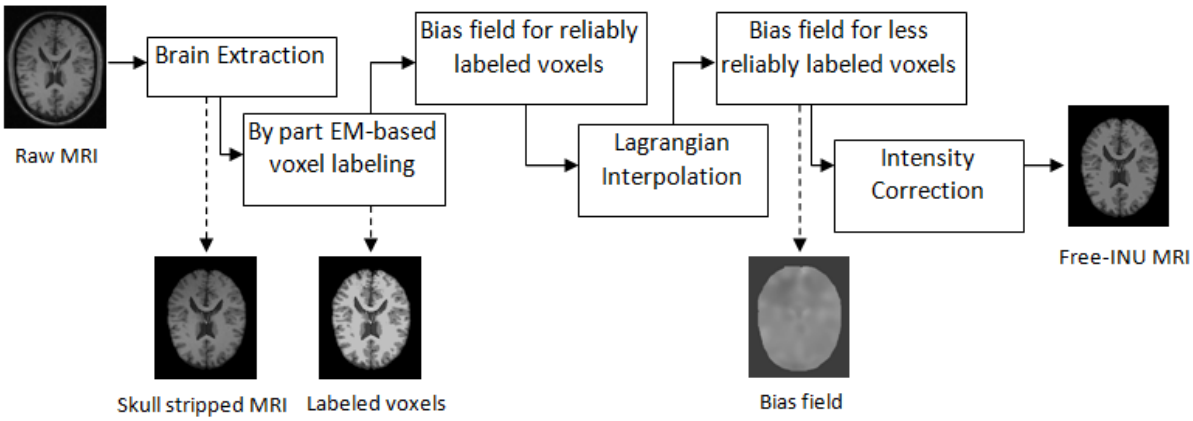

Figure 2. Processing steps according to the proposed method for bias field estimation and INU correction.

where only the brain tissues remain in the image; namely: CSF (Cerebro Spinal Fluid), GM (Gray Matter) and WM (White Matter). Considering the model for image formation cited above, it is not required that the image be denoised in order to perform the correction of the bias field. Indeed, the used bias represents the ratio between the noised measured image and the noised bias-free one (see Formula 1). Nevertheless, after the bias is corrected, it is suitable to denoise the image after assuming a noise model or by jointly image denoising and voxel labeling, as done in several works [12], given that prior global denoising could aggravate the partial volume effect problem, by which MR images are affected [2]. However, this issue is not included in our interest in this work.

By considering that MR data follows a Gaussian Mixture Model (GMM), the EM algorithm is well suited for both the estimation of the distribution parameters and image segmentation by voxel labeling. By taking into account the particularity of the bias field, that produces significantly different intensities for the set of voxels that belong to a same tissue, the EM clustering is performed for a set of sub-volumes, where the bias field is sufficiently weak in each sub-volume and then the resulting partitions are merged. In a sub-volume, noted *s*, there should exist the 3 classes of the brain tissues; namely, CSF, GM and

WM. The parameters to estimate by the EM algorithm for each tissue class T (T = 1, 2, 3) in the sub-volume s are the mean intensity μ^s_T and the standard-deviation σ^s_T. The probability density, assuming a Gaussian mixture, is given for a tissue class (T), by:

$$f_T(x_i;\ \mu_T^S, \sigma_T^S) = \frac{1}{\sigma_T^S\sqrt{2\pi}} e^{-\frac{1}{2}(x_i-\mu_T^S)/2{\sigma_T^S}^2} \tag{2}$$

According to this model, the adequacy of the voxel i to the tissue class T, which we consider as the membership certainty, is expressed as follows:

$$p_i^T = \frac{\pi_T f_c(x_i;\mu_T^S,\sigma_T^S)}{\sum_{j=1}^{k} \pi_T f_T(\bar{x}_j;\mu_j^S,\sigma_j^S)} \tag{3}$$

By using the adequacy probability, the distribution parameters are readjusted as follows:

$$\mu_T^S = \frac{1}{n_T^S}\sum_i p_i^T x_i \tag{4}$$

$$\sigma_T^S = \frac{1}{n_T^S}\sum_i p_i^T (x_\iota - \mu_T^S)^2 \tag{5}$$

$$\pi_T = \frac{n_T^S}{n^S} \tag{6}$$

where n^s and n^s_T are respectively the size of the set of all the voxels in the considered sub-volume s and the size of the cluster corresponding to the tissue class T in the same sub-volume.

To insure label integrity across the different sub-volumes, each one of the latter must contain all the considered labels (CSF, GM and WM). So, a sub-volume is set randomly within the global volume and after the EM clustering by parts is executed, the sub-volume will be retained only if the 3 labels are present. Otherwise, the sub-volume is rejected and another is randomly reset. As sub-volumes are randomly selected, a given voxel can be labeled several times according to the different sub-volumes to which it belongs. Also, the labels assigned to a same voxel may be different from a sub-volume to another. So, we calculated, for each voxel, the occurrences of labels assigned to it during sub-clustering that include the voxel. At the end of the clustering iterations, the label retained for a given voxel is that having maximum number of occurrences.

The following algorithm shows how the iterative clustering by parts is performed. We have opted for an

Algorithm 1 *Iterative EM Clustering by Parts()*

```
Inputs:  Skull stripped MRI volume
Outputs: Labels
for every voxel v in the MRI volume do
    for every label l do
        LabelOccurencies[v][l] ← 0
    end for
end for
NumberIterations ← 0
repeat
    repeat
        Subvolume ← random subvolume (xt, yt, zt, xb, yb, zb)
        Perform EM Clustering in Subvolume
    until Number of labels in Subvolume = 4 // background included
    for every voxel v in Subvolume do
        l ← label of v
        LabelOccurencies[v][l]++
    end for
    NumberIterations++
until NumberIterations = maxIterations
for every voxel v in the MRI volume do
        Labels[v] ← ArgMax_l(Label Occurencies[v][l], l ∈ [0..3]) // 0: background
end for
```

EM-based clustering instead of *k*-means one, because the former provides for every voxel the membership certainty to a given cluster. This certainty allows us to select only the voxels that certainly belong to their respective tissues. *K*-means clustering, which does not use a mixture of distributions, cannot quantify the membership certainty to the clusters and so does not allow to select reliably labeled voxels to fit the bias field.

As a result of this first stage, we obtain a segmentation of the image, where each voxel is assigned to a tissue class with its membership certainty. For each tissue class, the voxels that will be used to estimate the bias field are those with the membership certainty greater than a given threshold T_p, which will be set experimentally by using a set of MRIs with their respective group truth segmentation (see Section 4).

3.2 Bias Field Estimation and Intensity Correction

The intensity non-uniformity of the magnetic field leads to a disparity of the intensity values of the voxels belonging to the same tissue. It consists of a slow variation of the intensity according to an unknown model. So, the latter must be estimated in order that intensities can be corrected. In our work, we compute an initial voxel labeling in order to estimate the bias field and then correct the intensities. So, a coarse segmentation of the image is performed using an EM algorithm executed by parts in the global volume. After merging partial labeling results and the final labels affected to the image voxels, the bias field is estimated as a hyper-surface β, where $\beta(x,y,z)$ expresses the ratio between the mean intensity around the voxel (x,y,z) and the mean intensity at a voxel of reference (x_r,y_r,z_r) belonging to the same type of tissue and having the best membership certainty among all the voxels in the current sub-volume. We consider a neighborhood of 3×3 voxels around a given voxel to calculate the mean intensity value.

$$\beta(x,y,z) = \frac{\tilde{\hat{I}}(x,y,z)}{\tilde{\hat{I}}(x^r,y^r,z^r)} \tag{7}$$

where,

$$\tilde{\hat{I}}(x,y,z) = \frac{1}{|\chi(x,y,z)|}\sum_{i\in\chi(x_i,y_i,z_i)} \hat{I}(x_i,y_i,z_i) \tag{8}$$

where $\chi(x_i, y_i. z_i)$ is the set of neighboring voxels $\{(x_i, y_i, z_i)\}$ of (x, y, z) that belong to the same tissue.

For the previous treatment, we consider only the voxels $\{i\}$ that certainly belong to their respective tissue classes. A voxel i is retained for bias estimation, if its corresponding membership certainty, expressed by the probability p^{T_i} is greater than a given threshold T_p. For the rest of the voxels, the bias field is computed by interpolation using a Lagrangian hyper-surface [38] that we introduce in this work. The hyper-surface is computed using a set of voxels, sampled from those for which the bias field has been estimated. For each set of connected unlabeled voxels, for which we aim at computing the bias field, an including volume area is defined for this set. Within this volume, a set Ω of approximatively uniformly distributed labeled voxels are selected (see Figure 3(c)). This set is used as the control points to generate the Lagrangian hyper-surface, estimating the bias field in this area (see Figure 3(d)).

The Lagrangian interpolated hyper-surface, $\hat{\beta}(x,y,z)$ in an including volume area is expressed as follows:

$$\hat{\beta}(x,y,z) = \sum_{k\in\Omega} \beta_k \frac{\prod_{i\neq k}(x-x_i)(y-y_i)(z-z_i)}{\prod_{i\neq k}(x_k-x_i)(y_k-y_i)(z_k-x_i)} \tag{9}$$

where $\{(x_k, y_k, z_k) \in \Omega\}$ is the set of control points in the including volume area used to express the Lagrangian polynomial. Furthermore, a given point (x_k, y_k, z_k) is retained as a control point only if: first it was labeled belonging to one tissue and second its membership certainty is greater than the threshold T_p. Once the bias field is computed in the whole MRI volume, the voxel intensity $\hat{I^c}(x,y,z)$ at every voxel (x,y,z) of the volume is corrected as follows:

$$\hat{I^c}(x,y,z) = \hat{I}(x,y,z) \times \hat{\beta}(x,y,z) \tag{10}$$

The obtained corrected image $\hat{I^c}$ is considered bias field-free and it can be used for further processing, such as more accurate image segmentation or image registration.

Contrary to non-interpolation-based methods, such as B-spline-based ones [14], the proposed INU correction based on Lagrangian interpolation allows to preserve the values of the bias field at the reliably labeled voxels, considering that the latter are not affected by other artifacts, such as noise or partial volume effect. For less reliably labeled voxels, the bias field is estimated by the Lagrangian interpolation, resulting in a value better than the one directly calculated (according to Formula 7).

The overall proposed method can be expressed according to the following algorithm:

Algorithm 2 *INU Correction()*

Inputs: *MRI volume*
Outputs: *Free-INU Skull stripped MRI volume*

MRI Skull Stripping by BET
Labels ← EM-Clustering-by part (Skull Stripped MRI)
for *each connected part CP of homogeneous voxels in Skull stripped MRI* ***do***
  Set_1 *← Set of reliably labled voxels of CP*
  Set_2 *← Set of less reliably labeled voxels of CP //* Set_2 *=* $CP\text{-}Set_1$
  Compute the bias field B according formula 7 for the voxels in Set_1
  Compute Lagrangian polynome using bias fiels of all connected parts of Set_1 *(formula 9)*
  Estimate bias field of set_2 *using the computed Langrangian polynomial (using formula 9)*
end For
Correct the MRI INU for all the voxels by formula 10

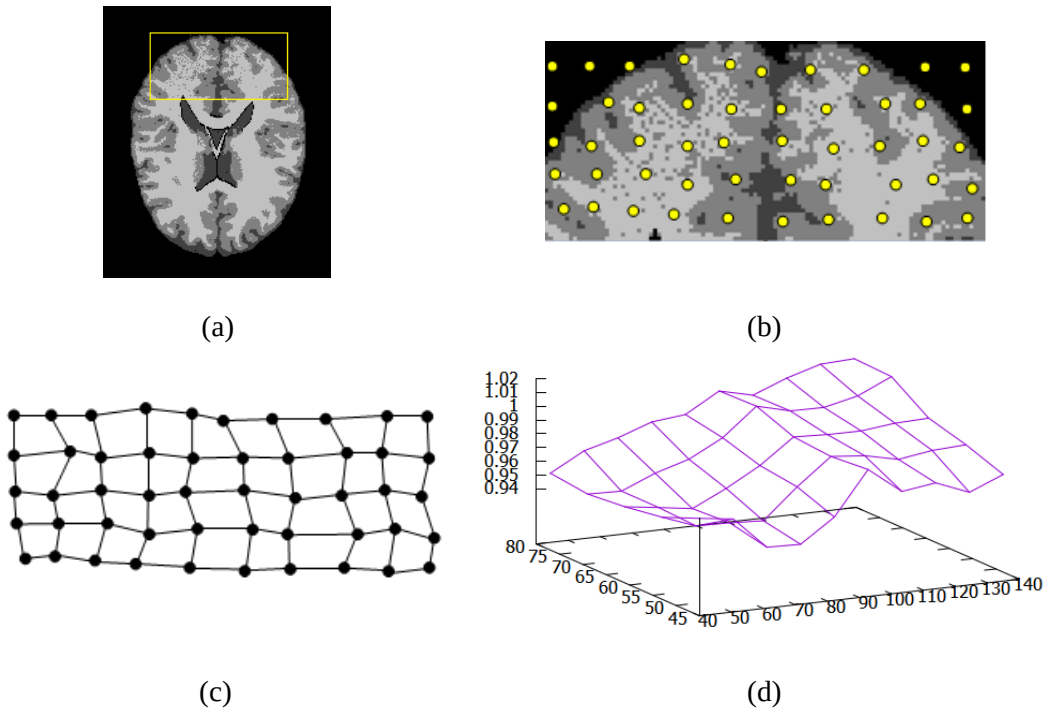

Figure 3. Selection of control points for fitting the hyper-surface: a) Slice from a clustered MRI, b) Point selection on 2D grid: for each regular position on the grid, the best voxel in the neighborhood are selected, having the highest membership certainty, c) Control points for Lagrangian interpolation, d) Bias field surface. The 3D surface is the projection of the 4D surface on the space (*X*,*Y*,*I*) corresponding to the 2D considered slice.

4. EXPERIMENTATION

We have experimented our method on simulated MRIs from the Brain Web database (https://brainweb.bic.mni.mcgill.ca) and on real MRIs from the Internet Brain Segmentation Repository IBSR database (https://www.nitrc.org/projects/ibsr). Simulated MRIs from the Brain Web were widely used in similar works, given that the Brain Web platform allows to customize artifact levels, in particular

INU. All used simulated MRIs are 181×217×181 voxels of size. Brain Web provides also ground-truth segmentation that allows us quantifying the efficiency of our method by comparing the segmentation results before and after bias field removal. We have considered several MRIs all with T1 modality. The INU in the considered MRIs ranges in {30%, 40% and 70%} and noise in {3% and 5%}. For real MRIs from IBSR database, all the 18 skull-stripped MRIs were considered. Each IBSR MRI is a volume of 256×256×128 voxels. We quantify the efficiency of the intensity correction by two different methods: First, by measuring the quality of the MRI segmentation by referring to its ground-truth segmentation provided by the used databases. Second, by measuring the coefficient of variation obtained for each image before and after bias field removal. For the first method, we use the overlap index kappa (κ). For a given tissue class T, it is expressed as: $\kappa_T = 2\times TP_T / (2\times TP_T + FP_T + FN_T)$, where TP_T, FP_T and FN_T are the numbers of respectively, correctly labeled voxels (true positives), voxels wrongly labeled as belonging to the tissue class T (false positives) and voxels wrongly labeled not belonging to the tissue class T (false negatives). Dice index expresses the overlap between the resulting segmentation and the ground truth segmentation, which expresses in turn several aspects, including accuracy. For the second method, the coefficient of variation is calculated as follows: $CV_T = \sigma_T/\mu_T$. It allows to estimate the variation amount around the mean value. When CV_T is low, the intensity non-uniformity is well corrected for the tissue class T.

4.1 Threshold Initialization

Only one threshold, T_p is used for our method for bias field estimation that we initialize experimentally by using a set of MRIs with their ground truth segmentation, as a learning set. The latter is composed of 6 MRIs, obtained by varying the couple (N%, INU%) in {1,3,5} x {20,60}. The optimal value of T_p corresponds to the maximum of the κ averages for the gray matter in the whole learning set.

Table 1. Initialization of the threshold T_p according to κ index for the training MR images.

T_p	0,50	0,55	0,60	0,65	0,70	0,75	0,80	0,85	0,90	0,95
κ	0,84	0,85	0,87	0,91	0,91	0,92	0,92	0,90	0,90	0,84

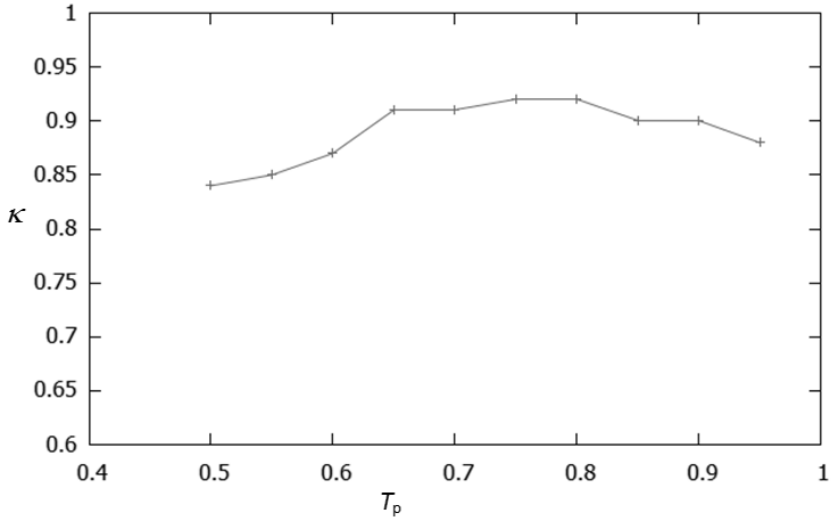

Figure 4. Average κ index according T_p threshold.

Table 1 and Figure 4 show the variation of the κ average for the gray matter. According the obtained results, T_p is set to 0.775.

4.2 Experimental Results

We consider only MRIs corresponding to healthy subjects, where the aim is to correct the INU after segmentation by extracting the three MRI tissues (CSF, GM and WM). To perform fully automatic segmentation, we should automatically set the tissue class T according to the tissue in which we have

interest. To do that, we take into account the knowledge that the cluster of the gray matter is the largest one and the cerebrospinal fluid is the smallest one (see Figure 5). The white matter cluster is in the middle [1].

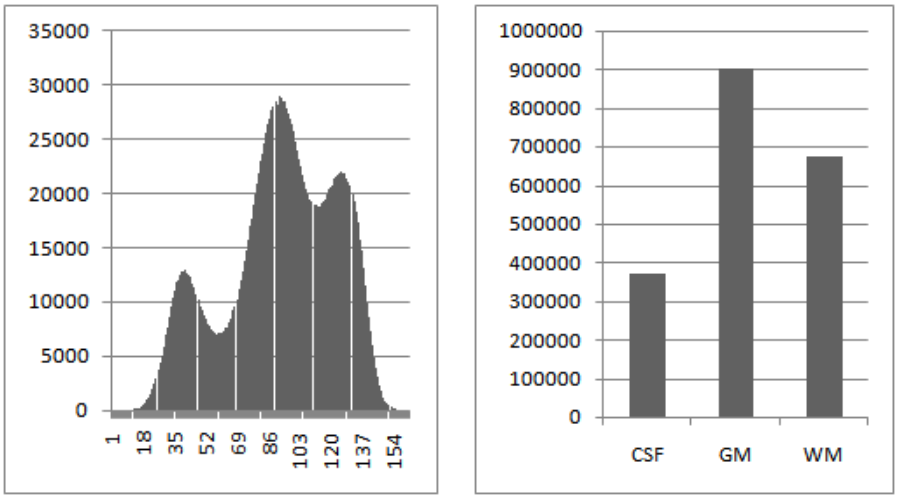

(a) (b)

Figure 5. Distributions of the intensities of an MRI: a) For a raw MRI : modes of the graphic, starting from left, correspond respectively to CSF, GM and WM, b) Distribution of the labels in the corresponding ground truth segmentation.

4.2.1 INU Correction Evaluation by Segmentation Comparison

Figure 6 shows the steps of the bias field correction and the obtained labeling of the tissues of interest: CSF, GM and WM. The MRI was generated by setting the noise level N% to 3 and the bias field INU% to 50. By observing images of EM clustering by parts (see sub-section 3.1), before and after bias field correction, we can see the set of voxels where the labels were corrected, in particular voxels at the top of the image after bias correction. The bias field in Figure 7 is a projection of the hyper-surface on the 3D space (X, Y, I), resulting in a conventional 3D surface.

Table 2. Dice coefficient for several MRIs obtained by different combinations of noise N% and intensity non-uniformity INU% before and after bias field correction.

		After bias correction		**Before bias correction**	
		N%=3	**N%=5**	**N%=3**	**N%=5**
INU%=30	Dice(WM)	93,87	92,60	90,82	88,43
	Dice(GM)	92,01	90,58	87,14	84,21
	Dice(CSF)	86,74	84,73	81,52	80,81
INU%=40	Dice(WM)	92,85	92,46	89,49	87,73
	Dice(GM)	92,01	90,58	87,14	84,21
	Dice(CSF)	84,21	82,76	79,63	78,93
INU%=70	Dice(WM)	91,52	90,94	87,34	85,15
	Dice(GM)	90,82	89,59	86,38	85,13
	Dice(CSF)	83,64	81,19	77,14	74,24

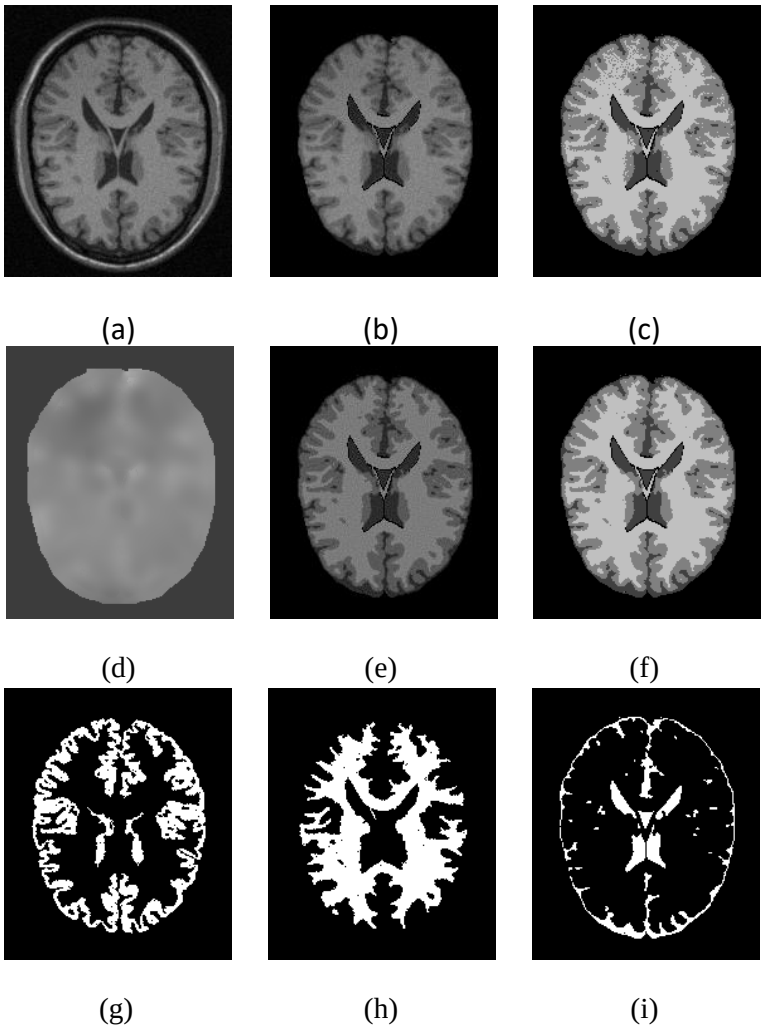

Figure 6. Steps for bias field correction : a) Raw MRI (before skull-stripping), b) Skull-stripped MRI, c) EM clustering before bias field correction, d) A slice from the bias field (projection) e) Brain after bias correction, f) EM clustering after bias field correction, g) Extracted GM, h) Extracted WM and i) Extracted CSF.

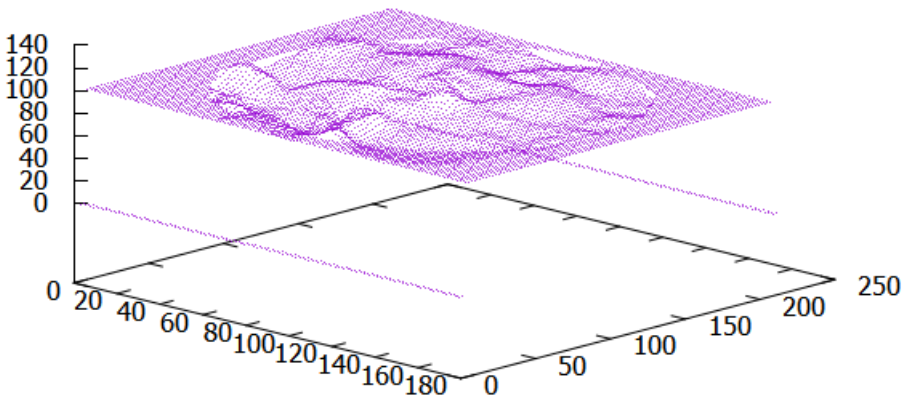

Figure 7. Projection of the bias field in the 3D space (*X*, *Y*, *I*) corresponding to a slice for which *Z* is fixed.

Table 2 and Figure 8 show how the bias field estimation and correction have allowed to enhance the labeling of the voxels in the different tissues. We can notice that for different combinations of noise level and INU level, the intensity disparity was corrected in the images even with high values of noise and INU, leading to better Dice coefficients.

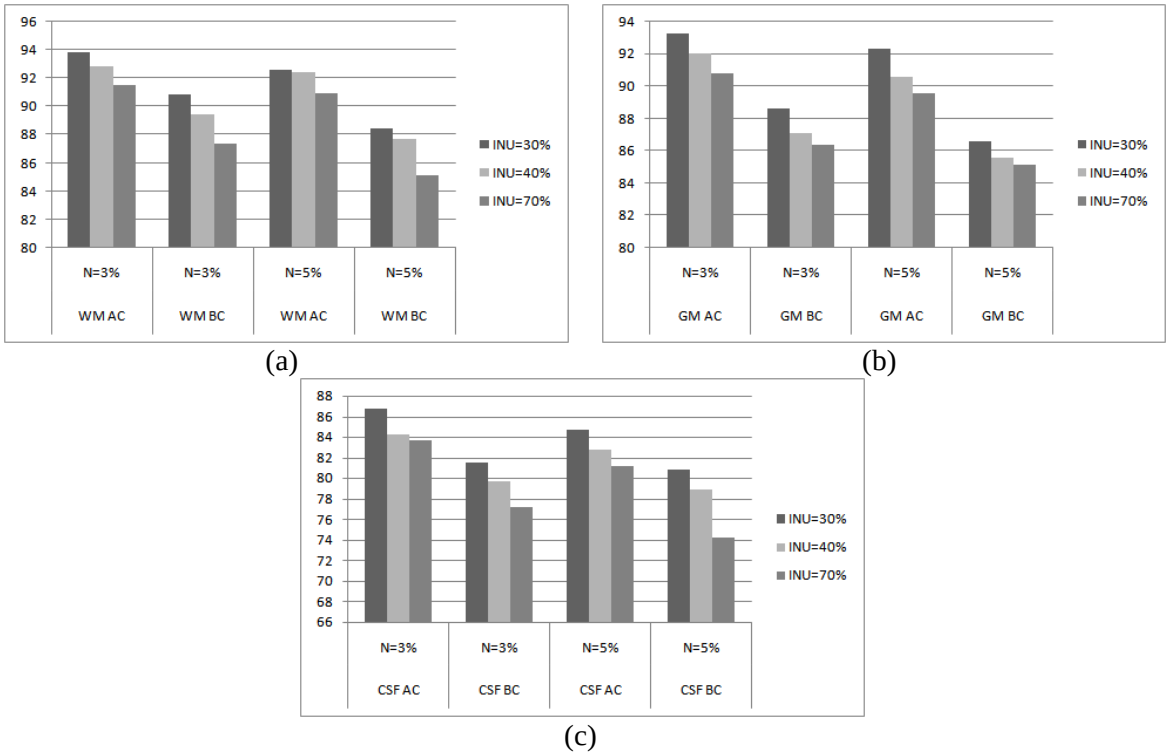

Figure 8. Dice coefficient according the different tissues and according to several artifact combinations (N% and INU%): a) WM before correction (BC) and after correction (AC) , b) GM (BC and AC) and c) CSF (BC and AC). For all the combinations, voxel labeling was significantly enhanced after the bias field was corrected.

4.2.2 Evaluation Using the Coefficient of Variation

Coefficient of variation is an indirect evaluation of performance of bias field correction [9], expressed as the fraction of the mean intensity μ_T of a given tissue class T to its standard deviation σ_T. For a tissue class T, it is expressed as follows:

$$CV_T = \frac{\sigma_T}{\mu_T}$$

Weak values of CV indicate a low bias field. So, when CV significantly decreases after bias field correction, that reflects a good performance of the used method. Furthermore, the coefficient of variation can be used as a metric to compare bias field correction methods.

Obtained results expressed by the coefficient of variation were compared to some well-referenced work in the literature. These are the works respectively of Ashburner and Friston [3], Guillemaud et al. [17], Gisper et al. [15] and Ardizzone et al. [2]. In the first work, the authors relied on surface fitting of the bias field after considering image data as a mixture model. In the second work, the authors combine homomorphism filtering and normalize convolution after operating a coarse segmentation to separate tissues from the image background. Gisper et al. presented a locally adaptive algorithm based on the minimization of the Classification Error Rate (CER) between different cerebral tissues. Finally, Ardizzone et al. used Homomorphic Unsharp Masking (HUM), which is a filtering technique for INU correction, without producing the Halo around the edges, resulting in a HUM-based halo compensation (HC-HUM). For comparison and as for the involved authors, we have considered different INU levels, which are respectively 20%, 40% and 70%. Table 3 and Figure 9 show the ranges of the coefficient of variation for the methods involved in the comparison and for the different levels of INU. For the different tissues (CSF, GM and WM) and for the different considered INU levels (20, 40 and 70%), the proposed method (Azz.) performs better than most of the methods involved in the comparison. Indeed, it performs better than the methods of respectively Ashburner et al., Guillemaud et al. and Gisper et al. for all the tissues and all the involved INU levels. Also, the proposed method performs better than that of Ardizzone et al. in 66% of cases (tissues and INU). We note here that using simulated MRIs from the Brain Web dataset, as most of the works which have dealt with the bias field in MRIs, allows well

understanding how MRIs are affected by the bias field and showing how bias field correction methods operate according to different levels of artifacts, in particular the bias field.

Table 3. Coefficient of variation obtained by the involved methods in the comparison, for different levels of INU.

INU level									
	20%			**40%**			**70%**		
Method	**CFS**	**GM**	**WM**	**CFS**	**GM**	**WM**	**CFS**	**GM**	**WM**
Gui. [17]	0,209	0,093	0,047	0,208	0,093	0,047	0,212	0,096	0,050
Ash. [3]	0,227	0,091	0,042	0,229	0,091	0,043	0,235	0,094	0,045
Gis. [15]	-	0,090	0,059	-	0,076	0,076	-	-	-
Ard. [2]	0,208	0,078	**0,022**	0,207	0,078	**0,022**	0,211	0,081	**0,024**
Azz. (proposed)	**0,193**	**0,073**	0,028	**0,195**	**0,075**	0,031	**0,203**	**0,079**	0,039

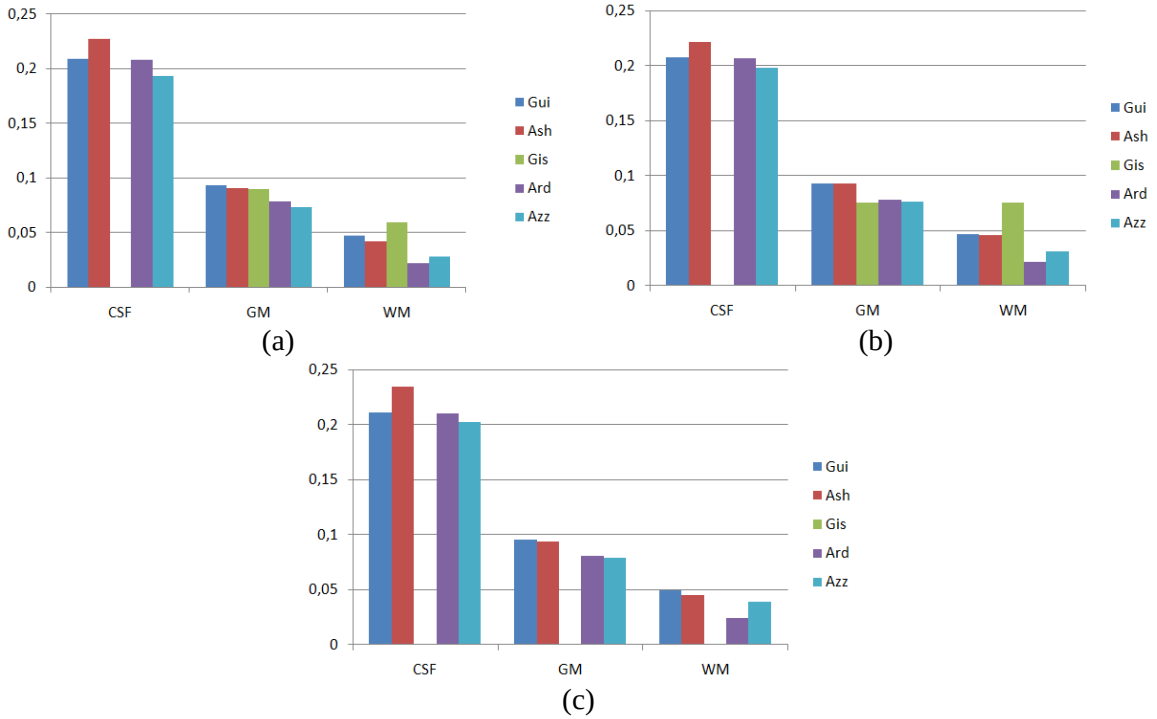

Figure 9. Coefficient of variation comparison for different levels of INU.

Considering real MRIs from IBSR, results of bias field correction, expressed by the coefficient of variation, were significantly enhanced. Figure 10 shows a sample of an IBSR MRI and the computed bias field. Figure 11 shows the CV values for the 18 skull-stripped MRIs. Obtained results for the 18 real MRIs, expressed by CV before and after correction, show that the bias field was significantly corrected for the whole images.

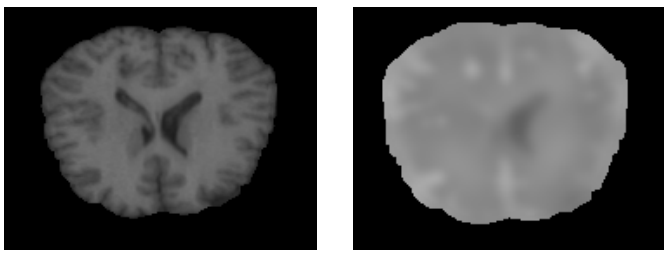

(a) (b)

Figure 10. Bias field in a sample of real IBSR MRI: a) Raw MRI, b) Computed bias field.

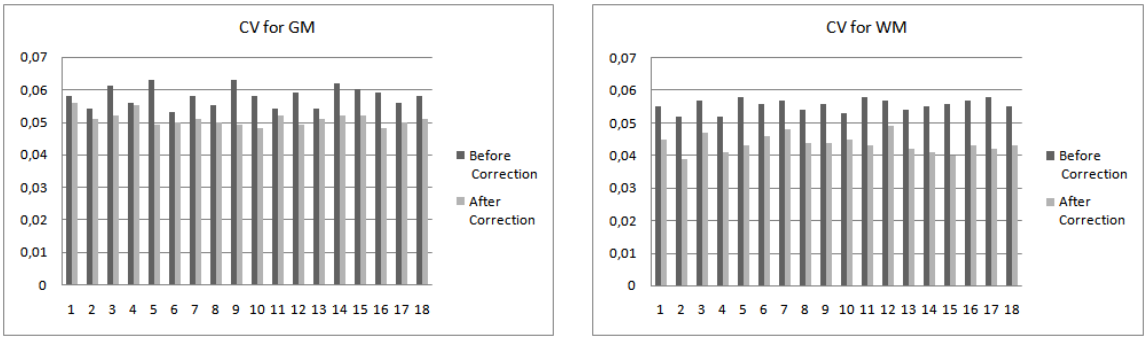

(a) (b)

Figure 11. CV with IBSR: a) Average CV before correction for the 18 MRIs of the IBSR dataset, b) Average CV after correction.

4.3 Analysis of Results and Discussion

Obtained segmentation results of noisy MRIs affected by different levels of intensity non-uniformity were significantly enhanced by the proposed method. In this work, we have opted for EM clustering performed by parts in several sub-volumes, in order to produce a fast and reliable labeling of voxels. However, any method that produces voxel labeling according to the anatomical tissues can be used on condition that it should define a membership certainty for voxel labeling. With the modified EM clustering algorithm proposed in this work, the remaining voxels for which the membership certainty is below the threshold T_p and the bias field was not initially estimated were not numerous. For such sets of voxels, it was always possible to define an including sub-volume that contains sufficiently voxels for which the bias field was calculated. The latter are used as control points for fitting a hyper-surface that will be used later to interpolate the bias field at the voxels less-reliably labeled. To contrast our method, we remind that most of the proposed methods for bias field modeling and intensity correction are Bayesian- or Markovian-based [36], [31]. They proceed by simultaneously compute the restored image I, the bias field β and the noise η, considering different priors. Others are optimization-based; such as those using some objective functions, expressing in most of the cases an energy function that must be minimized [28],[37]. For our case, we have opted for a first fast voxel labeling method that produces coarse image segmentation. The latter is used to estimate and correct the INU, then the final voxel labeling is performed using the corrected data. Furthermore, using high-reliably labeled voxels in order to fit the bias hyper-surface has allowed to obtain accurate interpolation for the voxels that are less-reliably labeled.

5. CONCLUSIONS

We have introduced in this paper a novel method for bias field estimation and correction in MR images. Computing the bias field is necessary to obtain enhanced segmentation results for such images. Contrary to B-spline approximation, we have opted for Lagrangian interpolation to estimate the bias field in the whole 3D data volume as a hyper-surface in a 4D space. Such a choice allows to accurately compute the bias field at the voxels that are reliably labeled and approximate it for the remainder voxels which are less reliably labeled. For that, we have introduced the membership certainty of voxel labeling to select the voxels which will be considered as control points for Lagrangian interpolation. The reliably labeled voxels allow computing a confident estimation of the bias field. Such enhancements were possible by introducing EM clustering by parts using several sub-volumes that allow to produce usable labeling even if the levels of the different artifacts are high in the MRI volume, in particular the INU level. Experimental results using several MRIs by considering different combinations of noise and INU levels and the comparison with other methods from the literature, showed the efficiency of the proposed method to estimate and correct the bias field in MR images. As most of methods for bias field correction in MRIs, our method does not consider ground-truth MRIs provided in different MRI databases. So, in future work, it is possible to consider other models for hyper-surfaces by integrating data and using machine learning methods. Furthermore, selecting reliable voxels for surface fitting was *ad hoc*, so a machine learning-based selection will enhance the accuracy of the computed hyper-surface that models the bias field.

REFERENCES

[1] E. D. Angelini, T. Song, B. D. Mensh and A. F. Laine, "Brain MRI Segmentation with Multiphase Minimal Partitioning: A Comparative Study," Int. J. Biomedical Imaging, vol. 2007, Article ID: 10526, pp. 1-15, 2007.

[2] E. Ardizzone, R. Pirrone, O. Gambino and S. Vitabile, "Illumination Correction on Biomedical Images," Computing and Informatics, vol. 33, no 1, pp. 175-196, 2014.

[3] J. Ashburner and K.J. Friston, "MRI Sensitivity Correction and Tissue Classification", NeuroImage, vol. 7, no. 4, DOI: 10.1016/S1053-8119(18)31539-8, 1998.

[4] J. Ashburner and K. J. Friston, "Unified Segmentation," NeuroImage, vol. 26, pp. 839-851, 2005.

[5] M. A. Balafar, A. R. Ramli, M. I. Saripan and S. Mashohor, "Review of Brain MR Image Segmentation Methods," Artificial Intelligence Review, vol. 33, no. 3, pp. 261-274, 2010.

[6] B. Caldairou, N. Passat, P. A. Habas, C. Studholme and F. Rousseau, "A Non-local Fuzzy Segmentation Method: Application to Brain MRI," Pattern Recognition, vol. 44, no 9, pp. 1916-1927, 2011.

[7] H. Chang, W. Huang, C. Wu, S. Huang, C. Guan, S. Sekar, K. K. Bhakoo and Y. Duan, "A New Variational Method for Bias Correction and Its Applications to Rodent Brain Extraction," IEEE Trans. Med. Imaging, vol. 36, no. 3, pp. 721-733, 2017.

[8] M. Qin and M. Chen, "A Brain MRI Bias Field Correction Method Created in the Gaussian Multi-scale Space," Proc. of the 9th International Conference on Digital Image Processing (ICDIP 2017), vol. 10420, pp. 1-8, Hong Kong, China, 2017.

[9] Z. Y. Chua, W. Zheng, M.W.L. Chee and V. Zagorodnov, "Evaluation of Performance Metrics for Bias Field Correction in MR Brain Images," J. of Magnetic Resonance Imaging, vol. 29, pp. 1271-1279, 2009.

[10] W. Cong, J. Song , K. Luan, H. Liang., L. Wang, X. Ma and J. Li, "A Modified Brain MR Image Segmentation and Bias Field Estimation Model Based on Local and Global Information," Journal of Computational and Mathematical Methods in Medicine, vol. 2016, Article ID: 9871529, pp. 1-13, 2016.

[11] X. Dai, Y. Lei, Y. Liu, T. Wang, L. Ren, W. J. Curran, P. Patel, T. Liu and X Yang, "Intensity Non-uniformity Correction in MR Imaging Using Residual Cycle Generative Adversarial Network," Journal of Physics in Medicine and Biology, vol. 65, no 21, p. 215025, 2020.

[12] I. Despotovic, B. Goossens and W. Philips, "MRI Segmentation of the Human Brain: Challenges, Methods and Applications, J. Comp. Math. Methods in Medicine, vol. 2015, Article ID: 450341, pp. 1-23, 2015.

[13] L. Dora, S. Agrawal, R. Panda and A. Abraham, "State-of-the-art Methods for Brain Tissue Segmentation: A Review," IEEE Reviews in Biomedical Engineering, vol. 10, pp. 235-249, 2017.

[14] E. Fletcher, O. Carmichael and C. DeCarli, "MRI Non-uniformity Correction through Interleaved Bias Estimation and B-spline Deformation with a Template," Proc. of the Annual International Conference of the IEEE Engineering in Medicine and Biology Society, pp. 106-109, San Diego, CA, USA, 2012.

[15] J. Gispert, S. Reig, J. Pascau, J. J. Vaquero, P. Garcia-Barreno and M. Desco, "Method for Bias Field Correction of Brain T1-weighted Magnetic Images Minimizing Segmentation Error," Human Brain Mapping, vol. 22, pp. 133-44, 2004.

[16] S. Gonzalez-Villa, A. Oliver, S. Valverde, L. Wang, R. Zwiggelaar and X. Llado, "A Review on Brain Structures Segmentation in Magnetic Resonance Imaging," Journal of Artificial Intelligence in Medicine, vol. 73, pp. 45-69, 2016.

[17] R. Guillemaud, "Uniformity Correction with Homomorphic Filtering on Region of Interest," Proc. of the Int. Conf. on Image Processing (ICIP98), (Cat. No.98CB36269), vol. 2, pp. 872-875, Oct. 1998.

[18] N. J. Habeeb, "Performance Enhancement of Medical Image Fusion Based on DWT and Sharpening Wiener Filter," Jordanian Journal of Computers and Information Technology (JJCIT), vol. 07, no. 02, pp. 118-129, June 2021.

[19] S. Kahali, S. Adhikari and J. K. Sing, "On Estimation of Bias Field in MRI Images: Polynomial *vs.* Gaussian Surface Fitting Method," Journal of Chemometrics, vol. 30, no. 10, pp. 602-620, 2016.

[20] C. Li, R. Huang, Z. Ding, C. Gatenby, D. N. Metaxas and J. C. Gore, "A Lvel Set Method for Image Segmentation in the Presence of Intensity Inhomogeneities with Application to MRI," IEEE Trans. Image Processing, vol. 20, no 7, pp. 2007-2016, 2011.

[21] J. Luo, Y. Zhu, P. Clarysse and I. E. Magnin, "Correction of Bias Field in MR Images Using Singularity Function Analysis," IEEE Trans. Med. Imaging, vol. 24, no. 8, pp.1067-1085, 2005.

[22] A. Madabhushi, J. K. Udupa and A. Souza, "Generalized Scale: Theory, Algorithms and Application to Image Inhomogeneity Correction," Comput. Vis. Image Underst., vol. 101, no. 2, pp.100-121, Feb. 2006.

[23] P.K., Mishro, S. Agrawal, R. Panda and A. Abraham, "Novel Fuzzy Clustering-based Bias Field Correction Technique for Brain Magnetic Resonance Images," IET Image Processing, vol. 14, no. 9, pp. 1929-1936, 2020.

[24] J. W. Murakami, C. E. Hayes and E. Weinberger, "Intensity Correction of Phased-array Surface Coil Images," Magnetic Resonance in Medicine, vol. 35, no. 4, pp. 585-590, 1996.

[25] P. A. Narayana and A. Borthakur, "Effect of Radio Frequency Inhomogeneity Correction on the Reproducibility of Intra-cranial Volumes Using MR Image Data," Magnetic Resonance in Medicine, vol. 33, no. 3, pp. 396-400, 1995.

[26] R. Prakash, R. Meena and R. S. S. Kumari, "Spatial Fuzzy C Means and Expectation Maximization Algorithms with Bias Correction for Segmentation of MR Brain Images," Journal of Medical Systems, vol. 41, no. 1, pp. 1-9, 2017.

[27] B. Scherrer, M. Dojat, F. Forbes and C. Garbay, "Agentification of Markov Model-based Segmentation: Application to Magnetic Resonance Brain Scans," Artificial Intelligence in Medicine, vol. 46, no. 1, pp. 81-95, 2009.

[28] X. Shan, X. Gong and A. K. Nandi, "Active Contour Model Based on Local Intensity Fitting Energy for Image Segmentation and Bias Estimation," IEEE Access, vol. 2018, no. 6, pp. 49817–49827, 2018.

[29] J. G. Sled and G. B. Pike, "Standing Wave and RF Penetration Artifacts Caused by an Elliptic Geometry: An Electrodynamics Analysis of MRI," IEEE Trans. Med. Imaging, vol. 17, no. 4, pp. 653-662, 1998

[30] S. M. Smith, "Fast Robust Automated Brain Extraction," Human Brain Mapping, vol. 17, no. 3, pp. 143-155, 2002.

[31] S. Song, Y. Zheng and Y. He, "A Review of Methods for Bias Correction in Medical Images," Biomedical Engineering Review, vol. 1, no. 1, DOI: 10.18103/bme.v3i1.1550, 2017.

[32] J. Song and Z. Zhang, "Brain Tissue Segmentation and Bias Field Correction of MR Image Based on Spatially Coherent FCM with Nonlocal Constraints," Comput. Math. Methods Medicine, vol. 2019, Article ID: 4762490, pp. 1-13, 2019.

[33] K. R. Sreenivasan, M. Havlicek and G. Deshpande, "Nonparametric Hemodynamic Deconvolution of FMRI Using Homomorphic Filtering," IEEE-Trans. Med. Imaging, vol. 34, no. 5, pp. 1155-1163, 2015.

[34] M. Styner, C. Brechbuhler, G. Szekely and G. Gerig, "Parametric Estimate of Intensity Inhomogeneities Applied to MRI," IEEE Trans. Med. Imaging, vol. 19, no. 3, pp. 153-165, 2000.

[35] P. Vemuri, E. G. Kholmovski, D. L. Parker and B. E. Chapman, "Coil Sensitivity Estimation for Optimal SNR Reconstruction and Intensity Inhomogeneity Correction in Phased Array MR Imaging," Proc. of the 19th International Conference on Information Processing in Medical Imaging (IPMI 2005), pp. 603-614, Glenwood Springs, USA, July 10-15, 2005.

[36] U. Vovk, F. Pernus and B. Likar, "A Review of Methods for Correction of Intensity Inhomogeneity in MRI," IEEE Transactions on Medical Imaging, vol. 26, no. 3, pp. 405-421, March 2007.

[37] L. Wang, J. Zhu, M. Sheng, A. Cribb, S. Zhu and J. Pu, "Simultaneous Segmentation and Bias Field Estimation Using Local Fitted Images," Pattern Recognition, vol. 74, pp. 145-155, 2018.

[38] A. I. Zayed and P. L. Butzer, "Lagrange Interpolation and Sampling Theorems," Non-uniform Sampling, pp. 123-168, DOI: 10.1007/978-1-4615-1229-5_3, Springer, 2001.

"A Hyper-surface-based Modeling and Correction of Bias Field in MR Images", D. Azzouz and S. Mazouzi.

ملخص البحث:

إنّ التّعامل مع العمليّات الاصطناعيّة في الصّور الطبّيّة أمر ضروري لأداء العديد من المهامّ، بما في ذلك التّجزئة. نقدّم في هذه الورقة طريقة مبتكرة لتصحيح حقل الانحياز في التّصوير بالرّنين المغناطيسي. فباستخدام نتائج التّجزئة التي يتمّ الحصول عليها عن طريق العنقدة المعدّلة المتعلّقة بتعظيم التّوقّع، تتمّ ملاءمة حقل الانحياز كسطح فوقيّ في حيّز كثير السّطوح رباعيّ الأبعاد.

بعد ذلك، يجري تصحيح حقل الانحياز بناءً على حقيقة أنّ النّقط المجسّمة التي تتبع للنّسيج نفسه يجب أن تكون لها شدّة الإضاءة نفسها في الصّورة كلّها. وهكذا، فبعد عملية سريعة وغير دقيقة لوسم النّقط المجسّمة عن طريق العنقدة تبعاً للأجزاء، يتم حساب حقل الانحياز للنّقط المجسّمة الموسومة بشكل موثوق. أمّا بالنسبة للنّقط المجسّمة الموسومة على نحوٍ أقلّ موثوقية، فإنّ حقل الانحياز يتم استيفاؤه باستخدام سطح فوقيّ يجري تقديره بواسطة استيفاء "لاجرانج" رباعي الأبعاد.

لقد قمنا بتقييم الطريقة المقترحة عن طريق مقارنة نتائج التّجزئة بوجود تصحيح حقل الانحياز وغياب تصحيحه. كذلك استخدمنا معامل التّغيّر ضمن حجم صورة الرّنين المغناطيسي. وكانت نتائج التقييم أفضل من حيث التّجزئة ومعامل التّغيّر – وبشكل ملموس- بعد تصحيح حقل الانحياز باستخدام الطريقة المقترحة.